# Ionomeric control of interchain interactions, morphology, and the electronic properties of conjugated polymer solutions and films

Thuc-Quyen Nguyen[a] and Benjamin J. Schwartz[b]
*Department of Chemistry and Biochemistry, University of California, Los Angeles, Los Angeles, California 90095-1569*

(Received 7 January 2002; accepted 18 February 2002)

It is becoming increasingly clear that the electronic properties of conjugated polymer films are strongly dependent on factors such as the conformation and the degree of aggregation of the polymer strands in the solution from which the film was cast. In this paper, we show how we can take advantage of conjugated ionomers (conjugated polymers that have been functionalized with side groups that can be electrically charged) to control the polymer morphology and degree of interchain interactions in both solutions and the films cast from them. The particular ionomer we study in this work, poly(2,5-bis[*N*-methyl-*N*-hexyl amino] phenylene vinylene) (BAMH-PPV), has dialkyl amino side groups that can be controllably charged by protonation with organic acids. In dilute BAMH-PPV solutions, protonation of just a few percent of the amino side groups leads to tight coiling of the polymer backbone, resulting in an enormous blueshift of the polymer's absorption and photoluminescence (PL) spectra. At higher BAMH-PPV solution concentrations, however, protonation of the side groups leads to redshifted emission, indicative of increased interactions between polymer chromophores that presumably result from counterion-mediated attractive interactions. The results suggest that conjugated polymer chromophores in solution interact by interpenetration of neighboring chains rather than by self-aggregation of the chromophores on a single chain. Scanning force microscopy experiments indicate that the surface topography of BAMH-PPV films varies directly with the degree of side-group protonation in the solution from which the film was cast. In addition, BAMH-PPV films cast from protonated solutions have a redder PL spectrum and a higher degree of exciton–exciton annihilation than films cast from neutral solutions, verifying that memory of the chain conformation and degree of chromophore interaction in solution carries through the spin-coating process. The charge-induced changes in the morphology of BAMH-PPV films also lead to dramatic differences in the performance characteristics of BAMH-PPV-based light-emitting diodes. Overall, we believe that the degree of control over the electronic properties of conjugated ionomers makes them attractive candidates for use in a wide variety of optoelectronic devices. © *2002 American Institute of Physics.*
[DOI: 10.1063/1.1468215]

## I. INTRODUCTION

Conjugated polymers are plastic semiconductors.[1] They have band gaps that can be tuned to any desired region of the visible spectrum by altering the chemical nature of either the polymer backbone or the side groups.[2,3] Because these materials can be dissolved in common solvents, it is straightforward to process conjugated polymers by printing or other techniques into easily patterned thin films for a variety of device applications.[4–7] This ease of processing, in combination with the many desirable mechanical properties of plastics, makes conjugated polymers quite attractive compared to inorganic semiconductors for a wide variety of applications. Indeed, high performance optoelectronic devices have been fabricated from conjugated polymers, including LEDs,[8,9] photovoltaic cells,[6,7,10] and transistors.[5,11,12]

Despite the large variety of potential applications, optimizing the performance characteristics of conjugated polymer-based devices is complicated by the molecular nature of these materials. Variations in how a conjugated polymer is processed can alter the way in which the polymer chains pack together. Changes in the chain packing, in turn, affect the bulk electronic properties of conjugated polymer films. The primary effect comes from the facts that conjugated polymer chains take on different conformations in different solution environments, and that the tendency for the conjugated chromophores to aggregate together depends sensitively on the chain conformation.[13,14] Both single molecule[15–17] and bulk film experiments[13] suggest that memory of the polymer conformation and degree of chromophore interaction is carried through the spin-casting process and survives into the film. This means that the film morphology, and hence, the performance of conjugated polymer-based devices, can be controlled by a number of solution processing factors, including: changing either the solvent or the concentration of the solution from which the polymer film is cast,[13,14,18] heating the solvent during poly-

[a]Present address: Department of Chemistry, Columbia University, New York, New York 10027.
[b]Electronic mail: schwartz@chem.ucla.edu

 

mer dissolution,[19] growing the films layer-by-layer using Langmuir–Blodgett[20,21] or self-assembly techniques,[22–24] altering the spin speed,[25,26] and annealing the films above the polymer's glass transition temperature.[13,27–30]

Why does changing the film morphology so strongly affect the performance of conjugated polymer-based devices? The electrical interactions caused by aggregation between conjugated polymer chromophores tend to promote good carrier transport through the film, but also reduce the luminescence quantum efficiency via the formation of interchain species such as excimers[13,31–34] or polaron pairs.[14,35,36] This leads to a fundamental trade-off in optimizing film morphology for light-emitting applications. To form emissive excitons, high carrier densities and mobilities are required, necessitating a large degree of $\pi$–electron interaction between the polymer chains in the device. Once the carriers recombine and the exciton is formed, however, minimal interchain contact is required to achieve the highest luminescence efficiency. Thus, the performance of conjugated polymer-based LEDs and other devices depends on the exact way in which the polymer chains are packed together.[13,27,37,38]

In this paper, we present a series of experiments designed to take advantage of the fact that the properties of a conjugated polymer film depend so sensitively on the morphology. The work centers on a new class of semiconducting polymers that have been functionalized with side groups that can be electrically charged in a controllable way: conjugated ionomers. Ionomers are polymers that contain a small number of easily ionizable side groups; in most applications, the solution $p$H is changed so that only a small fraction ($\leqslant 15$ mol %) of the side groups, which are usually randomly distributed along the polymer backbone, becomes charged.[39–41] The electrostatic forces involved can dramatically change the conformation of the polymer in solution as both the number of charges and the polarity of the solvent environment are varied. For example, in nonpolar liquids that are good solvents for an uncharged ionomer, the polymer chains will collapse and aggregate upon charging of the side groups to minimize exposure of the charges and counterions to the surrounding nonpolar environment.[42] In high-polarity solvents, on the other hand, charged ionomers can show the same kinds of behaviors exhibited by polyelectrolytes, ranging from chain extension due to self-repulsion of the charges along the backbone when the counterions are well solvated, to complete collapse of the polymer coil upon the addition of polyvalent counterions.[42,43] Nonconjugated ionomers have found a wide variety of applications, including use in improving charge injection at the electrodes of conjugated polymer-based devices.[44] Ionomeric control over the chain conformation of the conducting ionomer polyaniline also has been demonstrated by changing both the oxidation state of the backbone and the concentration of added salts.[45,46]

Our work focuses on controlling the conformation of the semiconducting conjugated ionomer poly(2,5-bis[*N*-methyl-*N*-hexyl amino] phenylene vinylene), or BAMH-PPV,[47,48] whose chemical structure is shown below in the inset to Fig. 1. BAMH-PPV is a phenylene vinylene-based conjugated polymer that has been functionalized with long-chain dialkyl amino groups to confer solubility in common organic solvents. This material has a solution-phase photoluminescence (PL) quantum yield of 79%,[19] which is the highest value we are aware of for a PPV-family polymer, giving it exceptional promise for application in light-emitting devices. The absorption and PL spectra of BAMH-PPV in dilute solution are presented below in Fig. 2(a). The spectra show that BAMH-PPV has electronic properties that are quite similar to those of its better-studied cousin, poly(2-methoxy-5-(2′-ethylhexyloxy)-1,4-phenylene vinylene), MEH-PPV, indicating that the amino side groups are similar to alkoxy side groups in their electron donating ability and in the degree of steric interactions they provide to break up the planarity of the PPV backbone. Unlike the alkoxy side groups in MEH-PPV, however, the dialkyl-amino side groups in BAMH-PPV can be easily protonated by the addition of acid, making it possible to use protonation as a ''knob'' to alter the solution conformation of the polymer without significantly affecting the electronic properties of the PPV backbone. As we will show, this provides an outstanding method for controlling the solution conformation and hence the morphology and electronic properties of conjugated polymer films.

Throughout the rest of this paper, we explore the relationship between morphology and the electronic properties of BAMH-PPV solutions and films as the polymer's conformation is altered by controllably charging the amino side groups. We find, using dynamic light scattering, that adding acid to protonate a small fraction of the BAMH-PPV side groups causes the polymer chains to tightly coil in nonpolar solvents. Steady-state and ultrafast photophysics experiments provide additional evidence for a decrease in conjugation length upon protonation at low polymer concentrations, and an increase in BAMH-PPV chromophore aggregation at high concentrations. The results suggest that interchromophore interactions result primarily from chain interpenetration rather than self-aggregation, and verify that the polymer's electronic properties in solution can be controlled directly by varying the amount of added acid. Scanning force microscopy experiments on BAMH-PPV films with different amounts of added acid show that the films' surface morphology (and hence the underlying chain packing) is correlated directly with the chain conformation and degree of aggregation in the solution from which the films are cast. Finally, we demonstrate how the charge-induced morphology changes in films affect the photophysics and performance of BAMH-PPV-based LEDs. Taken together, the results suggest that conjugated polymers with side groups whose charge is easily tuned will serve as ''next-generation'' materials because of the exquisite control they offer over the morphology and degree of interaction between polymer chains.

## II. EXPERIMENT

The BAMH-PPV used in this study, provided by Lindsay and Stenger-Smith, was synthesized according to standard procedures[47,48] that resulted in material with an average molecular weight of $\sim 60\,000$ g/mol as determined by gel permeation chromatography using polystyrene as a reference. Solution samples of BAMH-PPV were prepared by first dissolving the appropriate amount of polymer in *o*-xylene to

make a 1.0 %w/v solution. All solutions were heated at 40 °C for several hours while stirring to ensure the complete dissolution of the polymer, as discussed both in our previous work[19] and further below. The solutions were then divided into multiple portions, with differing amounts of camphor sulfonic acid (CSA) added to each portion. Typical CSA concentrations were 0, 1%, 3% and 7% weight camphor sulfonic acid to weight of BAMH-PPV. Given that the molecular weight of CSA (232.2 g/mole) is roughly 2/3 that of the BAMH-PPV repeat unit (328.2 g/mole), each percent by weight of added CSA corresponds roughly to 1.5 percent protonation of the polymer, assuming that every CSA molecule protonates a BAMH-PPV amino group. All sample processing, handling, and storage was carried out in the inert environment of a nitrogen glove box.

Film samples were prepared by spin-coating one of the BAMH-PPV solutions described above onto glass substrates (or for LEDs, ITO-coated glass substrates) at a spin speed of 1500 rpm. The spin-coated films were then heated at 50 °C for 2–3 h to ensure removal of the solvent. We took care to ensure that all the films used in this study were prepared identically; the only difference between films was the amount of CSA that had been added to the solution from which the film was cast. The spin-cast BAMH-PPV films had an optical density of ~1.0 at the absorption maximum of 475 nm, which with our measured sample absorbance of $6.86\times10^4$ OD/cm implies a film thickness of ~150 nm.

Optical and electrical measurements were carried out so that all the polymer samples were studied without ever having been exposed to ambient conditions. This was accomplished by placing the polymer samples into an optical cryostat (R. G. Hansen & Assoc.) within the glove box, sealing the cryostat, and then removing the sealed cryostat from the glove box. For film samples, the cryostat was evacuated prior to study, while solution samples were studied under nitrogen. UV-visible absorption spectra were measured using a spectrophotometer (Perkin-Elmer Lambda 25). To minimize the effects of self-absorption from optically dense samples, PL was collected from the front face of the film samples using a Fluorolog-3 (Instrument S. A. & Co.); solution PL quantum efficiencies were determined using Rhodamine 101 in ethanol as a standard with assumed unit quantum yield.[49] For the femtosecond pump–probe experiments on films, the laser pulses passed through the transparent substrate to minimize simultaneous exposure of the sample to light and any potential ambient gases.[13,50] All the pump–probe scans presented below were completely reproducible, and we saw no signs of irreversible sample damage[13,51] at laser fluences below 50 $\mu$J/cm$^2$, even for samples studied in air. Details of our ultrafast laser apparatus have been provided elsewhere.[13] For BAMH-PPV LEDs, a ~100-nm thick, ~1 mm$^2$ 10:1 Mg:Ag electrode capped with ~100 nm of Ag was evaporated on top of the spin-cast polymer film; details of the LED fabrication and characterization are also provided elsewhere.[27]

Topographic images of the BAMH-PPV film samples were obtained using a scanning force microscope (Park Scientific) with 100 $\mu$m scanners. The scanning force microscopy (SFM) experiments were done in the air at room temperature in contact mode with an applied loading of 1–1.5 nN using a scanning frequency between 0.5 and 1 Hz.[52] Dynamic light scattering measurements were performed on a Microtrac ultrafine particle analyzer (Leeds & Northrup). For both dynamic light scattering and SFM measurements, the conditions were similar to those used in our previous work on both BAMH-PPV[19] and other conjugated polymers.[13,53]

## III. RESULTS AND DISCUSSION

In previous work, we explored the properties of unprotonated BAMH-PPV chains, and determined that the way in which unprotonated BAMH-PPV is dissolved significantly affects the electronic properties of the chains in solution as well as the photophysics and device performance of the resultant films.[19] We found that even after stirring for 2 days, the polymer is not completely dissolved: instead, BAMH-PPV solutions stirred at room temperature behave more as a suspension of small pieces of polymer film, showing solid-state effects such as exciton–exciton annihilation.[54] The films cast from such incompletely dissolved solutions have a rough, agglomerated morphology, and LEDs fabricated from these films have low electroluminescence (EL) efficiencies. Heating the BAMH-PPV solutions to 50 °C for a few hours while stirring greatly improves the dissolution and produces films with a smooth topography and high EL efficiencies. Once the polymer is fully dissolved, however, we also found that additional heating of the solution produced films with a higher degree of interchain interactions, as evidenced by increased exciton–exciton annihilation and higher operating currents/lower EL efficiencies compared to films cast from unheated, fully dissolved solutions. All the results suggest that understanding the details of how conjugated polymers (and BAMH-PPV in particular) are dissolved in solution is critical to being able to reproducibly fabricate and optimize conjugated polymer-based devices.[19] In the work reported here, we extend these previous observations to BAMH-PPV chains that have been controllably protonated. Throughout this work, we have taken care to ensure that all our BAMH-PPV solutions were fully and identically dissolved without being subject to excess heating.

### A. Controlling the conformation of conjugated ionomers in solution

One of the basic properties of ionomers is that altering the charge density along the polymer backbone can control the polymer's solution conformation. The most direct evidence for this comes from dynamic light scattering, which measures the diffusion constant of the polymer, thus determining the coil size (radius of hydration) from the Stokes–Einstein equation and the measured solution viscosity.[55] Because of polydispersity in the molecular weight of the polymer and fluctuations in how the chains fold, there is typically a distribution of coil sizes.[56] The upper panel in Fig. 1 compares the coil size distributions from dynamic light scattering experiments on both protonated (7% w/w CSA) and unprotonated (neutral) dilute ($\leq$0.1% w/v) BAMH-PPV solutions. The solid curve shows that the average size of the diffusing species is ~17 nm in the neutral solution. The small tail to higher sizes likely is due to aggregation, which causes a small group of polymer chains to

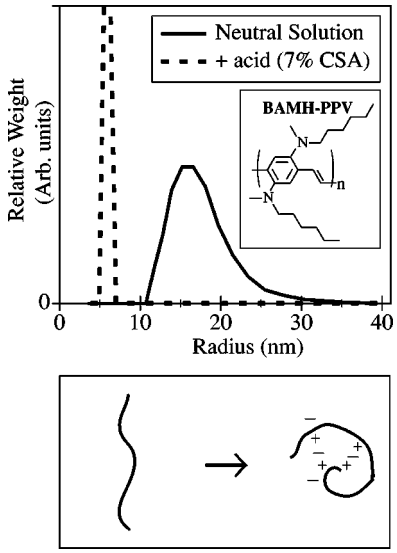


FIG. 1. Relationship between protonation and chain conformation in solution. Top panel: Dynamic light scattering size distributions (hydrodynamic radii) for dilute neutral (solid curve) and protonated (7% w/w CSA, dashed curve) solutions of BAMH-PPV. The inset shows the chemical structure of BAMH-PPV. Lower panel: Schematic illustration of the conformational change of a charged ionomer in nonpolar solution. Protonation increases the charge along the backbone of the open chain coil, causing the coil to collapse to minimize exposure of the both the backbone charges and counterions to the nonpolar environment. See the text for details.

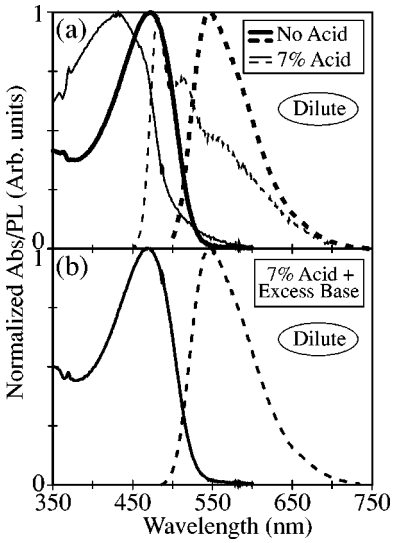


FIG. 2. Reversible effects of protonation on the electronic structure of dilute BAMH-PPV solutions. (a) Normalized UV-visible absorption (solid curves) and PL (dashed curves) for dilute solutions of BAMH-PPV. The thick curves show the results for an unprotonated solution, while the thin curves show the results for a protonated (7% w/w CSA) solution. (b) Normalized UV-visible absorption (solid curve) and PL (dashed curve) for the same protonated solution used to generate the thin curves in panel (a) following the addition of excess triethylamine base.

diffuse as a single entity: this type of coil size distribution is typical for fully dissolved neutral BAMH-PPV chains with this molecular weight in a good solvent like *o*-xylene.[19] The dashed curve shows that upon protonation of the polymer, the average solution coil size shrinks to only ~6 nm, and the size distribution becomes significantly narrower relative to the neutral polymer solution. The smaller size of the protonated polymer chains clearly results from the addition of CSA, which causes the charged BAMH-PPV chains to fold in the nonpolar solvent environment, as depicted for a generic ionomer in the lower panel of Fig. 1. The narrowing of the size distribution upon protonation indicates that the process of coiling the newly charged chains tends to break up any loose BAMH-PPV aggregates that existed before charging, so that all the charged chains have similar diffusion constants. The question we address next is how this change in conformation upon protonation affects the photophysics of BAMH-PPV in solution.

Figure 2(a) shows the absorption (solid curves) and fluorescence spectra (dashed curves) of very dilute (~0.005% w/v) BAMH-PPV solutions with (thin curves) and without (thick curves) added CSA (7% w/w). It is clear that one effect of protonation is an increase in the vibronic structure and the addition of a red tail to the PL spectrum of BAMH-PPV. We believe that the red tail results from an electrostatically induced aggregation of the polymer chromophores, as discussed further below. It is not entirely clear why protonation also produces an increase in vibronic structure. One possibility is that the PL of the protonated polymer comes from chromophores with a more homogeneous distribution of conjugation lengths than the PL from neutral BAMH-PPV. This might result if the distribution of conjugation lengths narrows in a similar fashion upon protonation as the distribution of polymer coil sizes, as seen in Fig. 1. The increased vibronic structure might also result from enhanced energy transfer: the tighter protonated chain coil should bring a greater range of chromophores within the Förster radius of a given excitation, providing more through-space pathways for excitons to migrate to low-energy sites along the polymer backbone.[15–17,57,58] This type of Förster energy funnel in the protonated polymer would result in most of the PL coming from a few low-energy chromophores instead of from a broad distribution of high- and low-energy chromophores as in unprotonated BAMH-PPV.

In addition to the increased vibronic structure and red tail, Fig. 2(a) shows that the most evident effect of adding acid on the polymer's electronic structure is a very large blueshift ($\geqslant$50 nm) of the protonated polymer's absorption and PL spectra relative to those of neutral BAMH-PPV. One possibility is that this blueshift is caused by a reduction in the electron-donating ability of the amino side groups upon protonation. If this were the case, however, the fact that only a few percent of the amino side groups are protonated would lead us to expect a broadening of the absorption and PL spectra: different chromophores would have different numbers of protonated amino groups and thus different degrees of charge donation to the backbone $\pi$ system. The fact that the spectrum does not undergo significant broadening (as evidenced by the sharp vibronic structure) leads us to assign the blueshift to the reduction in average conjugation length caused by the tight coiling: the additional twists and kinks required to coil the chain lead to a large decrease in the average extent of $\pi$–electron conjugation along the backbone. Such kinks and twists of the polymer backbone are also associated with emission quenching defects, and indeed,

the change in polymer conformation induced by acid is also reflected in the PL quantum yield: in these dilute solutions, the PL quantum yield is 79% for neutral BAMH-PPV but drops to only 35% upon protonation. At least part of this sharp drop in PL quantum efficiency upon acidification may result from enhanced energy transfer, which provides more through-space pathways for energy to migrate to quenching centers or other defects.

While it is likely that the conformational change of BAMH-PPV upon protonation causes the PL quenching, the drop in emission quantum yield might also be due to some type of irreversible chemical change induced by the acid. For example, the acid could oxidize the PPV backbone rather than simply protonate one of the amino side groups. To investigate this possibility, we added a base, triethylamine (TEA), to see if it was possible to neutralize the protonated BAMH-PPV amino groups. Figure 2(b) shows that both the absorption (solid curve) and emission (dashed curve) spectra of the protonated BAMH-PPV solutions shift back to the red upon the addition of excess TEA. A comparison of the spectra in Fig. 2(b) to the thick curves presented in Fig. 2(a) shows that treatment with excess base can reverse the effects of acid addition: the spectra of the BAMH-PPV solutions following addition of CSA and then excess TEA are nearly identical to those of freshly dissolved, unprotonated BAMH-PPV. This result supports the conclusion that protonation changes only the polymer's conformation and does not cause irreversible chemical damage to the polymer backbone. The fact that the conformational change is reversible also opens new possibilities for future work: for instance, one could imagine treating a film comprised of tightly coiled, protonated BAMH-PPV chains with excess base to selectively change just the conformation of the chains at the interface that will be in direct contact with the electrode in an optoelectronic device.

The data in Fig. 2 were measured from solutions of BAMH-PPV that are very dilute, so that aggregation of the polymer chains is highly unlikely. Most conjugated polymer films, however, are cast from high-concentration solutions that have high viscosities to ensure uniform coverage when spin-coating. A wide variety of work indicates that aggregation and interchain electrical interactions increase greatly as the concentration of a conjugated polymer solution is increased toward the typical $\geqslant 1\%$ w/v used for spin-coating.[53,59,60] Figure 3 presents the PL spectra of concentrated (1% w/v) BAMH-PPV solutions with (solid curve) and without (dashed curve) the addition of 7% w/w CSA.[61] Unlike what is observed in dilute protonated solutions [Fig. 2(a)], the PL of high-concentration protonated BAMH-PPV solutions has an extended red tail and is redshifted relative to that of the neutral polymer. The presence of this type of weak, redshifted emission is the classic spectral signature of interchain interactions: when two or more polymer chain segments pack together in an aggregated, $\pi$-stacked configuration, the electronic wave function can be delocalized over multiple chromophores.[13,32,62–65] Direct assignment of the redshifted PL from the high-concentration protonated BAMH-PPV solutions, however, is complicated for two reasons. First, self-absorption at high concentration suppresses the blue portion of the emission, making accurate determination of the shape of the PL spectrum difficult. Second, there is no simple way to quantify the competition between the expected emission blueshift from the decreased conjugation length and the expected emission redshift from increased chromophore aggregation. The fact that a redshift is observed, however, verifies that protonation at high concentrations is correlated with some degree of increased interchain interactions, such as excimer or polaron pair formation.

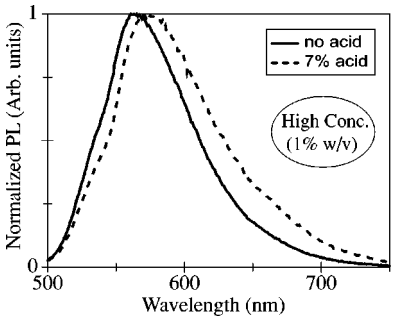


FIG. 3. Effects of protonation on the electronic structure of BAMH-PPV at high concentrations. Normalized front-face collected PL spectra for 1% w/v solutions of neutral (solid curve) and protonated (7% w/w CSA, dashed curve) solutions of BAMH-PPV.

If the aggregation of BAMH-PPV chromophores at high concentrations is increased upon protonation, then we would expect to see a drop in the PL quantum efficiency as the concentration of acid is increased. Direct measurement of the PL quantum yield in high-concentration solutions, however, is problematic because there is no good way to account for the effects of self-absorption. Thus, we elected to measure the PL quantum yield of our high-concentration BAMH-PPV solutions indirectly by using time-resolved spectroscopy. Figure 4 displays the results of femtosecond pump–probe experiments on both protonated and neutral high-concentration BAMH-PPV solutions. The samples were excited at 475 nm and the excited state lifetime probed via stimulated emission at a wavelength of 590 nm. The excitation intensity was chosen to be low enough to ensure that the measured lifetimes were not affected by exciton–exciton

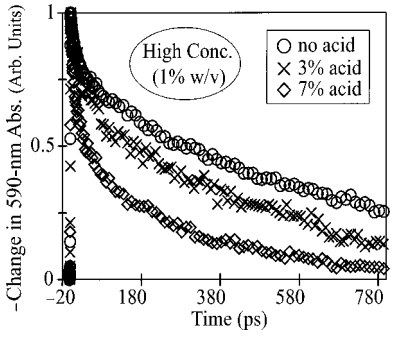


FIG. 4. Effects of protonation on the excited-state lifetime of BAMH-PPV at high concentration. The symbols show the magnitude of the stimulated emission at 590 nm following 480-nm excitation of 1.0% w/v solutions of BAMH-PPV: neutral solution (circles); 3% w/w CSA protonated solution (crosses); and 7% w/w CSA protonated solution (diamonds). The three data sets have been normalized to the same absolute magnitude for ease of comparison.

annihilation.[13,19] Single exponential fits to the data in Fig. 4 show that the lifetime of the high-concentration neutral solution is $670 \pm 15$ ps, which drops to $430 \pm 10$ ps upon the addition of 3% w/w CSA and to $240 \pm 10$ ps when the CSA concentration is raised to 7% w/w. In our previous work, we measured a 1.18 ns PL lifetime and a 79% PL quantum yield for unprotonated BAMH-PPV in dilute solutions, establishing that the radiative lifetime of BAMH-PPV is 1.49 ns.[19] Thus, the measured BAMH-PPV lifetimes in the high-concentration neutral, 3%, and 7% CSA solutions correspond to PL quantum yields of 45%, 29% and 16%, respectively. The much lower emission quantum yield in the high-concentration neutral solution (45%) compared to the dilute neutral solution (79%) makes it clear that simply increasing the polymer concentration leads to chromophore aggregation that quenches the emission. Adding acid to the solutions causes a further decrease in the lifetime, which could be the result of the protonation induced decrease in conjugation length, a conformationally or electrostatically-induced increase in chromophore aggregation, or both. Although the lifetime measurements alone cannot distinguish which of the two mechanisms dominates the emission quenching, the redshift of the PL upon protonation suggests that a significant fraction of the quantum yield reduction is the result of protonation-induced aggregation.

The idea that changing the conformation or electrostatics of a conjugated polymer can lead to aggregation is in line with other reports in the literature. For example, McBranch and co-workers observed an increase in chromophore aggregation of the conjugated polyelectrolyte poly(2-methoxy-5-propyloxy sulfonate) phenylene vinylene (MPS-PPV) upon addition of the divalent cation methyl viologen and surfactant.[66] The fact that methyl viologen both is a good electron acceptor and helps to promote aggregation of the MPS-PPV chromophores leads to ''superquenching'' (a single quencher eliminating the emission from multiple chromophores) of the MPS-PPV fluorescence, opening the possibility for applications in biosensing.[66,67] Bazan and co-workers have found an even greater superquenching of MPS-PPV oligomers by methyl viologen in the presence of surfactants, suggesting enhanced aggregation of the oligomeric chromophores.[68] Other groups have observed the signatures of chromophore aggregation (redshifted emission and decrease in PL quantum yield) when the solubility of PPV-based polymers is decreased either by changing the temperature,[69,70] solvent,[18,53,60] or by the addition of nonsolvents[14,59,71,72]

Although lowering the temperature, the addition of nonsolvents and the electrical charging of side groups all lead to tighter coiling of a conjugated polymer chain, the correlation between chain coiling and chromophore aggregation is not so simple. In previous work, we found less chromophore aggregation for MEH-PPV dissolved in tetrahydrofuran (THF) than dissolved in chlorobenzene, despite a smaller polymer coil size in THF.[53] The data in Figs. 1 and 2 are also suggestive of little chromophore aggregation in dilute solutions of tightly coiled BAMH-PPV chains: the dynamic light scattering results in Fig. 1 suggest that physical polymer aggregates are broken up upon coiling, and the net emission blueshift seen in Fig. 2 indicates little contribution to the PL from interchain species [although the red PL tail in Fig. 2(a) does suggest a small degree of aggregation] upon protonation. In combination, these results imply that conjugated polymers are stiff enough that their chromophores do not easily self-aggregate in solution, even when the chains are relatively tightly coiled. Instead, we believe that many factors are involved in the ability of conjugated polymer chromophores to aggregate. For instance, both lowering the temperature and the addition of nonsolvents not only reduce the polymer coil size, but also bring polymer solutions closer to the theta condition.[73] Even through the tightly coiled chains in low-concentration polymer solutions near the theta condition do not interact, approaching the theta condition at higher concentrations can lead to an increase in the overlap of neighboring polymer strands.[74] Thus, the aggregation of conjugated polymer chromophores in poor solvents[14,59,71,72] may be the result of increased interchain penetration rather than self-aggregation from tight folding.

In addition to chain interpenetration, the electrostatic forces that control the conformation of polyelectrolytes and ionomers also could play a direct role in chromophore aggregation. For example, the protonation of BAMH-PPV in high-concentration solutions produces a large concentration of counterions, which can create electrostatically mediated attractions between adjacent chromophores that are not present at lower concentration.[75,76] The fact that protonation increases attractive forces between chains is borne out by the observation that BAMH-PPV is no longer soluble in nonpolar solvents like *o*-xylene in the presence of high concentrations of acid ($\geqslant 10\%$ w/w). Overall, it is clear that the nature of conjugated polymer chromophore aggregation in solution depends on a subtle interplay of many factors, including the polymer coil size, the nature of the polymer–polymer and polymer–solvent interactions, the degree of chain overlap and electrostatics.

### B. Controlling the morphology of conjugated ionomer films

Given that electrostatic forces allow us to control both the conformation and the degree of aggregation of conjugated ionomers in solution, the question we address next is how well memory of the solution properties carries through the spin-casting process to influence the properties of conjugated ionomer films. Both Huser & Yan[15,16] and Barbara and co-workers[17,77] have performed elegant experiments which demonstrate that the optical properties of single conjugated polymer molecules vary with preparation conditions, a direct result of changes in the way the individual polymer molecules are folded. Correlating the measured electronic properties with the local chain geometry is difficult, however, because there is no simple method to measure chain conformation and packing in a solid-state polymer sample: even techniques such as x-ray diffraction[18,78] and transmission electron microscopy[79] that usually reveal morphological details provide almost no molecular information when applied to amorphous conjugated polymer films. The most straightforward technique for accessing the structure of polymer films is SFM, which measures the surface topography of the

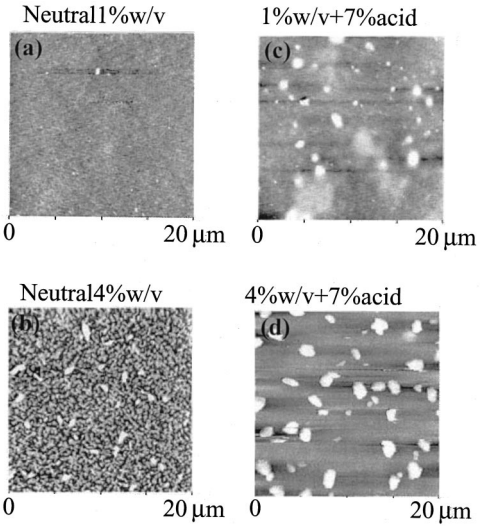


FIG. 5. Effects of protonation on the surface topography of BAMH-PPV films. Each panel shows a $(20\ \mu m)^2$ scanning force micrograph of a BAMH-PPV film cast from a high-concentration solution similar to those studied in Figs. 3 and 4. Counterclockwise from upper left: (a) Film cast from neutral 1% w/v solution; the black-to-white color scale represents a height difference of ~4 nm. (b) Film cast from neutral 4% w/v solution; the black-to-white color scale represents a height difference of ~35 nm. (c) Film cast from a protonated (7% w/w CSA) 1% w/v solution; the black-to-white color scale represents a height difference of ~15 nm. (d) Film cast from a protonated (7% w/w CSA) 4% w/v solution; the black-to-white color scale represents a height difference of ~150 nm.

packed polymer chains. In previous work, we were able to use a combination of SFM and near-field scanning optical microscopy (NSOM) to make a direct correlation between topographic features on the surface of MEH-PPV films and regions with increased chromophore aggregation.[80,81] This verified that the surface topography measured by SFM is directly related to the underlying molecular chain packing.

Figure 5 presents scanning force micrographs of BAMH-PPV films cast from high-concentration solutions like those whose spectroscopy was explored in Figs. 3 and 4. All the images cover a 20-×20-μm area, but the color height scale in each image is different. The images show that the surface topography of BAMH-PPV films changes dramatically when the concentration of the polymer is increased or when acid is added to the solution from which the film is cast. The surface of the film cast from the neutral 1% w/v solution shown in Fig. 5(a) is quite smooth (the black to white color change represents a height difference of ~4 nm), suggesting that the film is formed by the uniform spreading of individual polymer chains from the solution. When the concentration of the neutral polymer solution is increased to 4% w/v, however, the surface of the resulting film shows topographic features (''bumps''), suggestive of large tangled regions of polymer chains [Fig. 5(b), in which the black to white color scale corresponds to a ~35 nm height difference]. The spectroscopic data in the previous section demonstrate clearly that there is increased aggregation of the polymer chromophores in solution at higher polymer concentrations. Thus, we have evidence for a direct correlation between the degree of chromophore aggregation in solution, determined spectroscopically, and the presence of large, tangled regions of polymer chains in films. The images in Figs. 5(a) and 5(b) are consistent with a picture in which the conjugated polymer aggregates that form by interpenetration of adjacent chains in solution can survive the spin-casting process and persist into the film.[13]

Given this apparent relationship between polymer aggregation in solution and the morphology of the resultant film, we expect the chain packing in BAMH-PPV films to be dramatically altered by protonation of the polymer in solution. This is verified by the scanning force micrographs of the surfaces of films cast from protonated BAMH-PPV solutions, which are shown in Figs. 5(c) and 5(d). The black to white color scale represents a height change of ~15 nm for the film cast from a 1% w/v solution with 7% w/w CSA [Fig. 5(c) and ~150 nm for the film cast from a 4% w/v solution with 7% w/w CSA Fig. 5(d)]. The protonated films are rough on many length scales, with bumps whose height is roughly half the color scale in each image. We have already argued in the previous section that protonation of BAMH-PPV in high-concentration solutions promotes chain aggregation, presumably due to a counterion-mediated electrostatic attraction between chains.[76] Figure 5 suggests that aggregated clumps of chains in films cast from high-concentration protonated BAMH-PPV solutions form because memory of the tangling and interpenetration of the polymer chains in solution (even though they are tightly folded) survives the spin-coating process. The films cast from unprotonated solutions, in contrast, have less chain interpenetration and form primarily by uniform spreading of individual polymer chains.

The scanning force micrographs in Fig. 5 show clearly that the physical structure of BAMH-PPV films changes with the degree of chain aggregation in the solutions from which the films were cast; the question we address next is how this change in morphology affects the films' electronic structure. The UV-visible absorption and PL spectra of the BAMH-PPV films (not shown; see Ref. 19) strongly resemble those of the solutions from which they were cast, suggesting a similar degree of chromophore aggregation between solution and film. In particular, the film spectra show a significant redshift upon protonation, similar to that observed in Fig. 3, again consistent with preservation of the interchain electronic structure through the casting process. Additional information concerning the electronic properties of the films comes from time-resolved spectroscopic experiments, which provide a more sensitive probe of interchain interactions. The open square symbols in Figs. 6(a) and 6(b) show the results of low-intensity femtosecond pump–probe stimulated emission experiments on the BAMH-PPV films cast from 7%-protonated and neutral 1% w/v solutions, respectively; these experiments were performed on the same films whose scanning force micrographs were shown in Figs. 5(a) and 5(c). The trend in the excited state lifetimes of the films mirrors that of the solutions from which they were cast (cf. Fig. 4): the emission lifetime of the film cast from neutral solution is relatively long (~200 ps), while the emission of the film cast from the protonated solutions is significantly quenched ($\leqslant$100 ps). This same type of relationship between the steady-state spectra of solutions and the films cast from them was also observed in our previous work on

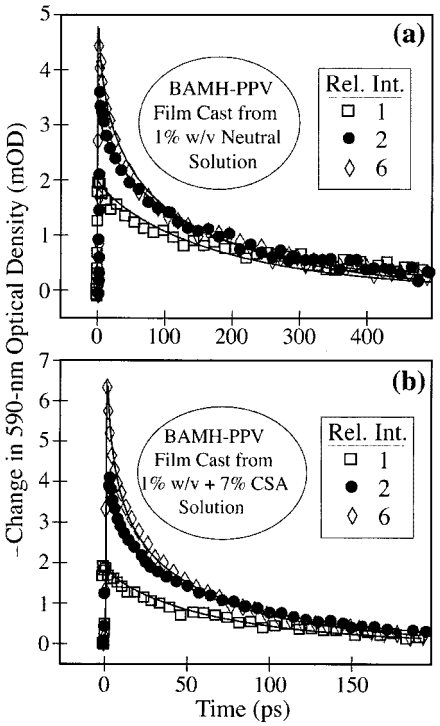


FIG. 6. Effects of protonation on the intensity dependence of the excited-state lifetime of BAMH-PPV films. In both panels, the data show the magnitude of the 590-nm stimulated emission following 480-nm excitation of BAMH-PPV films, normalized to the same maximum change in absorbance for ease of comparison. The squares show the data taken at the lowest excitation fluence ($\sim 4\ \mu J/cm^2$), while the filled circles and diamonds are taken at excitation fluences 3 and 6 times higher, respectively. Panel (a) shows the data for a BAMH-PPV film cast from a neutral 1% w/v solution; panel (b) shows the data for a protonated (7% w/w CSA) 1% w/v solution. The solid curves in both panels are global fits of the data for each film to Eq. (1) (see the text for details).

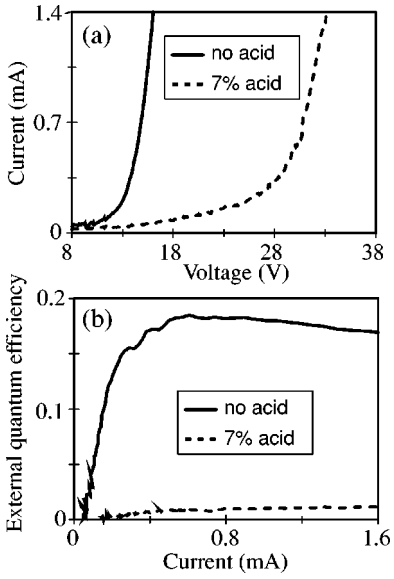


FIG. 7. Effects of protonation on the behavior of ITO/BAMH-PPV/Mg:Ag LEDs. In both panels, the solid curves show the results for LEDs in which the active BAMH-PPV layer was cast from a neutral 1% w/v solution, while the dashed curves are for LEDs with the active BAMH-PPV cast from a 7% w/w CSA protonated 1% w/v BAMH-PPV solution. (a) Current versus applied bias voltage for the LEDs. (b) External electoluminesnce quantum efficiency (in percent photons/electron) versus current for the LEDs.

MEH-PPV,[13,53] verifying that the electronic properties of conjugated polymer films can indeed be controlled by the electronic properties of the polymer in solution.

To confirm that the observed lifetime difference in the BAMH-PPV films is the result of different degrees of interchromophore interactions, we also examined how the emission lifetime changes as a function of excitation intensity. It is well known that the emission lifetime decreases at high excitation densities due to exciton–exciton annihilation,[50,51,54,82,83] as described by

$$\frac{dN(t)}{dt} = -\frac{N(t)}{\tau} - \frac{\beta}{\sqrt{\tau}} N^2(t), \tag{1}$$

where $N(t)$ is the time-dependent population density of emissive excitons [with the density of excitons at time zero, $N(0)$, directly proportional to the intensity of the excitation pulse], $\tau$ is the exciton lifetime, and $\beta$ is the bimolecular recombination coefficient.[84] We demonstrated in previous work on MEH-PPV that the ease with which exciton–exciton annihilation can occur, as measured by the magnitude of $\beta$, is a direct function of the degree of contact between the polymer chromophores:[13] after all, excitons cannot easily encounter one another to annihilate if the chains are not in contact.[85] The data in Fig. 6(a) show how the emission dynamics of a neutral BAMH-PPV film changes as the excitation intensity is varied over a factor of 6; Fig. 6(b) shows the dynamics of a protonated BAMH-PPV film for the same excitation intensities. For both films, there is a clear decrease in the emission lifetime at higher excitation intensities, as expected for exciton–exciton annihilation. The data also show that the lifetime of the protonated film decreases faster at higher intensities than that of the neutral film. The solid curves though the data points in Fig. 6 are global fits of the emission data for each film to Eq. (1). The fits give values of $\tau$ and $\beta$ of 210 ps and $2.7\times10^{-19}$ $cm^3/\sqrt{ps}$ for the neutral film, and 85 ps and $5.4\times10^{-19}$ $cm^3/\sqrt{ps}$ for the protonated film, respectively.[86] Both the decreased value of $\tau$ and the increased value of $\beta$ are direct signatures of increased chromophore interaction in the protonated BAMH-PPV film relative to the neutral BAMH-PPV film.[13] Thus, Fig. 6 provides strong evidence that the electrical charging of conjugated ionomers enhances the electronic interactions between polymer chromophores in both solutions and the films cast from them.

The final question we investigate is how the ionomerically controlled change in BAMH-PPV film morphology affects the performance of light-emitting devices based on this material. Figures 7(a) and 7(b) display current-voltage ($I-V$) and brightness-voltage ($L-V$) curves for ITO/BAMH-PPV/Mg:Ag sandwich structure LEDs in which the active BAMH-PPV layer was cast under the same conditions as the films studied in Figs. 5 and 6. The devices fabricated from the protonated solutions have a higher injection threshold voltage, lower working current, and lower light output than their counterparts based on the neutral solutions. This is a direct result of the change in conformation and packing of the polymer chains upon acidification of the casting solution.

The protonated films are comprised of domains of highly interpenetrating chains that are loosely agglomerated together: within each domain, the chains are in good electrical contact, but there is poor electrical connectivity between domains. The rough surface morphology of the protonated films [Figs. 5(b) and 5(d)] also suggests poor electrical contact with the cathode,[27] which in combination with the poor interdomain contact results in the observed low injection current [Fig. 7(a)]. Figure 7(b) shows that the devices based on protonated films also have lower electroluminescence quantum efficiency of the devices based on films cast from neutral solutions: independent of current, the neutral device's EL efficiency (solid curve) is ~25% higher than that of the devices based on 3%-added CSA cast films (not shown), and ~70% higher than devices built from 7%-added CSA cast-films (dashed curve). This result reflects the fact that carrier recombination in the protonated films most likely takes place within an aggregated domain, where the presence of large numbers of interchromophore electronic species leads to a reduced emission quantum yield.[13,27,37] Clearly, controlling the chain conformation and degree of aggregation is critical to the production of efficient conjugated polymer-based optoelectronic devices.

## IV. CONCLUSIONS

In summary, we have shown that it is possible to use electrical charges to control the conformation and degree of aggregation of conjugated polymers in both solutions and the films cast from them. In dilute solutions of the ionomer BAMH-PPV, protonation of the side groups leads to a reversible tight coiling of the polymer chains and a decrease in chain aggregation. Although the decreased PL quantum yield suggests that the tightly coiled chromophores may experience enhanced Förster energy transfer, the large blueshift of both the absorption and PL spectra indicates that the tight chain coiling does not result in significant direct interactions between the chromophores on a single polymer molecule. Increasing the polymer concentration, however, produces a redshifted PL spectrum that is characteristic of interchromophore interactions, presumably the result of increased interpenetration of adjacent polymer chains. The degree to which electrical interactions can take place between conjugated polymer chromophores depends on a subtle interplay between polymer–polymer forces, polymer–solvent forces, and the Coulomb forces between any charged side groups and their counterions in solution.

As with other conjugated polymers, the polymer conformation and degree of chromophore aggregation of conjugated ionomers in solution is largely preserved through the spin-casting process, resulting in control over the morphology and electrical properties of conjugated ionomer films. Scanning force microscopy verifies that both the concentration and the degree of protonation of the ionomer in solution directly affect the surface topography of the resultant film. A variety of optical experiments suggests that the electrical properties of conjugated ionomer films mirror those of the solutions from which they were cast. In particular, the presence of enhanced exciton–exciton annihilation at high excitation intensities upon protonation of BAMH-PPV verifies that the degree of chromophore interactions in films can be controlled by charging the polymer chains. The differences in the electrical properties of ionomer films cast under different conditions are readily apparent in the behavior of ionomer-based LEDs. The clumped chain morphology of the charged ionomer films leads to both poor electrical conductivity and poor electroluminescence efficiency, consistent with the picture of the solution conformation and degree of aggregation persisting into the film.

Although the results presented above show that simply charging the side groups and coiling the chains can be detrimental to device performance, we believe that the morphological control offered by conjugated ionomers will lead to significant advances in the optimization of conjugated polymer-based devices. The direction our research is headed is to use the electrical charges along the ionomer backbone to cause the conjugated chains to self-assemble and pack with a desired morphology. Our hope is that we will be able to produce conjugated polymer films that are optimized for different applications simply by spin-coating from solutions with the appropriate charge conditions, such as the addition of acid or the use of polar solvents and added salts. If successful, this approach would allow easy fabrication of a wide variety of devices, without the need for complex assembly processes such as layer-by-layer growth or monolayer compression on a Langmuir trough. We speculated above on the prospects of using the reversibility of the conformational change upon protonation as a means to selectively change the polymer morphology at the electrode interface, a process which could clearly benefit device performance.[27] We are also planning experiments to explore the effects of thermal annealing on conjugated ionomer films, in which the charged side groups could direct the chain packing in the polymer melt into structures not accessible using standard conjugated polymers. With control over a wide range of conformations and hence electrical properties, we believe that conjugated ionomers are the materials of the future for the production of organic optoelectronic devices.

## ACKNOWLEDGMENTS

We thank Geoff Lindsay and John Stenger-Smith for providing the BAMH-PPV and camphor sulfonic acid used in this work, and Jingling Yang and Mark Thompson for assistance with the LED fabrication and characterization. We are also grateful to Chuck Knobler for use of the scanning force microscope and to Fred Wudl for use of fluorimeter. We are indebted to Alex D. Smith for assistance in measuring the thickness of a series of films to determine the optical absorption depth of BAMH-PPV, and to Ignacio B. Martini for assistance with the exciton–exciton annihilation calculations. This work was supported by grants from the National Science Foundation (No. DMR-9971842), the Petroleum Research Fund of the American Chemical Society (No. 37029-AC5,7), and the Energy Sciences and Technology Program of the University of California Energy Institute. B.J.S. is a Cottrell Scholar of Research Corporation, an Alfred P. Sloan Foundation Research Fellow, and a Camille Dreyfus Teacher-Scholar.

[1] R. H. Friend, R. W. Gymer, A. B. Holmes *et al.*, Nature (London) **397**, 121 (1999).
[2] A. Kraft, A. C. Grimsdale, and A. B. Holmes, Angew. Chem. Int. Ed. Engl. **37**, 402 (1998).
[3] U. Mitschke and P. Bauerle, J. Mater. Chem. **10**, 1471 (2000).
[4] J. Bharathan and Y. Yang, Appl. Phys. Lett. **72**, 2660 (1998).
[5] H. Sirringhaus, T. Kawase, R. H. Friend, T. Shimoda, M. Inbasekaran, W. Wu, and E. P. Woo, Science **290**, 2123 (2000).
[6] S. E. Shaheen, R. Radspinner, N. Peyghambarian, and G. E. Jabbour, Appl. Phys. Lett. **79**, 2996 (2001).
[7] M. Granstrom, K. Petritsch, A. C. Arias, A. Lux, M. R. Andersson, and R. H. Friend, Nature (London) **395**, 257 (1998).
[8] J. H. Burroughes, D. D. C. Bradley, A. R. Brown, R. N. Marks, K. Mackay, R. H. Friend, P. L. Burns, and A. B. Holmes, Nature (London) **347**, 539 (1990).
[9] G. Gustafsson, Y. Cao, G. M. Treacy, F. Klavetter, N. Colinari, and A. J. Heeger, Nature (London) **357**, 477 (1992).
[10] C. J. Brabec, N. S. Sariciftci, and J. C. Hummelen, Adv. Func. Mat. **11**, 15 (2001).
[11] A. J. Lovinger and L. J. Rothberg, J. Mater. Res. **11**, 1581 (1996).
[12] H. E. A. Huitema, G. H. Gelinck, J. B. P. H. van der Putten, K. E. Kuijk, C. M. Hart, E. Cantatore, P. T. Herwig, A. J. J. M. van Breemen, and D. M. de Leeuw, Nature (London) **414**, 599 (2001).
[13] T.-Q. Nguyen, I. Martini, J. Liu, and B. J. Schwartz, J. Phys. Chem. B **104**, 237 (2000).
[14] P. Wang, C. J. Collison, and L. J. Rothberg, J. Photochem. Photobiol., A **144**, 63 (2001).
[15] T. Huser and M. Yan, J. Photochem. Photobiol., A **144**, 43 (2001).
[16] T. Huser, M. Yan, and L. J. Rothberg, Proc. Natl. Acad. Sci. U.S.A. **97**, 11 187 (2000).
[17] J. Yu, D. H. Hu, and P. F. Barbara, Science **289**, 1327 (2000).
[18] S. H. Lim, T. G. Bjorklund, and C. J. Bardeen, Chem. Phys. Lett. **342**, 555 (2001).
[19] T.-Q. Nguyen, R. Y. Yee, and B. J. Schwartz, J. Photochem. Photobiol., A **144**, 21 (2001).
[20] M. I. Sluch, C. Pearson, M. C. Petty, M. Halim, and I. D. W. Samuel, Synth. Met. **94**, 285 (1998).
[21] J. Kim and T. M. Swager, Nature (London) **411**, 1030 (2001).
[22] J.-D. Hong, D. Kim, D. Cha, and J.-I. Jin, Synth. Met. **84**, 815 (1997).
[23] R. Schroeder, J. R. Heflin, H. Wang, H. W. Gibson, and W. Graupner, Synth. Met. **121**, 1521 (2001).
[24] M. F. Durstock, B. Tayler, R. J. Spry, L. Chiang, S. Reulbach, K. Heitfeld, and J. W. Baur, Synth. Met. **116**, 373 (2001).
[25] Y. Shi, J. Liu, and Y. Yang, J. Appl. Phys. **87**, 4254 (2000).
[26] J. Liu, Y. Shi, L. Ma, and Y. Yang, J. Appl. Phys. **88**, 605 (2000).
[27] T.-Q. Nguyen, R. C. Kwong, M. E. Thompson, and B. J. Schwartz, Appl. Phys. Lett. **76**, 2454 (2000).
[28] T. W. Lee, O. O. Park, L. M. Do, and T. Zyun, Synth. Met. **117**, 249 (2001).
[29] T.-W. Lee and O. O. Park, Appl. Phys. Lett. **77**, 3334 (2000).
[30] J. I. Lee, G. Klaerner, and R. D. Miller, Synth. Met. **101**, 126 (1999).
[31] S. A. Jenekhe and J. A. Oseheni, Science **265**, 765 (1994).
[32] R. Jakubiak, C. J. Collison, W. C. Wan, L. J. Rothberg, and B. Hsieh, J. Phys. Chem. A **103**, 239 (1999).
[33] I. D. W. Samuel, G. Rumbles, C. J. Collison, R. H. Friend, S. C. Moratti, and A. B. Holmes, Synth. Met. **84**, 497 (1997).
[34] E. M. Conwell, Phys. Rev. B **57**, 14 200 (1998).
[35] M. Yan, L. J. Rothberg, E. W. Kwock, and T. M. Miller, Phys. Rev. Lett. **75**, 1992 (1995).
[36] M. Yan, L. J. Rothberg, F. Papadimitrakopoulos, M. E. Galvin, and T. M. Miller, Phys. Rev. Lett. **72**, 1104 (1994).
[37] P. L. Burn, R. Beavington, M. J. Frampon, J. N. G. Pillow, and I. D. W. Samuel, Mater. Sci. Eng., B **85**, 190 (2001).
[38] X. L. Chen, A. J. Lovinger, Z. N. Bao, and J. Sapjeta, Chem. Mater. **13**, 1341 (2001).
[39] A. Eisenberg, Macromolecules **3**, 147 (1970).
[40] S. Nomula and S. L. Cooper, Macromolecules **30**, 1355 (1997).
[41] K. Chakrabarty, R. A. Weiss, A. Sehgal, and T. A. Seery, Macromolecules **31**, 7390 (1998).
[42] R. D. Lundberg and R. R. Phillips, J. Polym. Sci., Polym. Phys. Ed. **20**, 1143 (1982).
[43] W. M. Gelbart, R. F. Bruinsma, P. A. Pincus, and V. A. Parsegian, Phys. Today **53**, 38 (2000).
[44] T. W. Lee, O. O. Park, L. M. Do, T. Y. Zhung, T. Ahn, and H.-K. Shim, J. Appl. Phys. **90**, 2128 (2001).
[45] M. Angelopoulos, R. Dipietro, W. G. Zheng, A. G. MacDiarmid, and A. J. Epstein, Synth. Met. **84**, 35 (1997).
[46] W. Zheng, M. Angelopoulos, A. J. Epstein, and A. G. MacDiarmid, Macromolecules **30**, 7634 (1997).
[47] J. D. Stenger-Smith, P. Zarras, L. H. Merwin, S. E. Shaheen, B. Kippelen, and N. Peyghambarian, Macromolecules **31**, 7566 (1998).
[48] J. D. Stenger-Smith, W. P. Norris, A. P. Chafin, and S. T. Sackenger, U.S. Patent 5,604,292 (1998).
[49] I. B. Berlman, *Handbook of Fluorescence Spectra of Aromatic Molecules*, 2nd ed. (Academic, New York, 1984).
[50] G. J. Denton, N. Tessler, N. T. Harrison, and R. H. Friend, Phys. Rev. Lett. **78**, 733 (1998).
[51] V. I. Klimov, D. W. McBranch, N. N. Barashkovb, and J. P. Ferraris, Chem. Phys. Lett. **277**, 109 (1997).
[52] J. Fang, M. Dennin, C. M. Knobler, Yu. Godovsky, N. N. Makarova, and H. Yokoyama, J. Phys. Chem. B **101**, 3147 (1997).
[53] T.-Q. Nguyen, V. Doan, and B. J. Schwartz, J. Chem. Phys. **110**, 4068 (1999).
[54] R. G. Kepler, V. S. Valencia, S. J. Jacobs, and J. J. McNamara, Synth. Met. **78**, 227 (1996).
[55] B. Berne and R. Pecora, *Dynamic Light Scattering with Applications to Chemistry, Biology and Physics* (Wiley, New York, 1976).
[56] C. L. Gettinger, A. J. Heeger, J. M. Drake, and D. J. Pine, J. Chem. Phys. **101**, 1673 (1994).
[57] T.-Q. Nguyen, J. Wu, V. Doan, S. H. Tolbert, and B. J. Schwartz, Science **288**, 652 (2000).
[58] B. J. Schwartz, T.-Q. Nguyen, J. Wu, and S. H. Tolbert, Synth. Met. **116**, 35 (2001).
[59] R. Chang, J. H. Hsu, W. S. Fann, J. Yu, S. H. Lin, Y. Z. Lee, and S. A. Chen, Chem. Phys. Lett. **317**, 153 (2000).
[60] M. Zheng, F. Bai, and D. Zhu, J. Photochem. Photobiol., A **116**, 143 (1998).
[61] At concentrations this high, making a similar comparison for UV-visible absorption spectra is impossible because of the extremely large optical density of the solutions.
[62] U. Lemmer, S. Heun, R. F. Mahrt, U. Scherf, M. Hopmeier, U. Siegner, E. O. Gobel, K. Mullen, and H. Bessler, Chem. Phys. Lett. **240**, 373 (1995).
[63] J. W. Blatchford, S. W. Jessen, L.-B. Lin, T. L. Gustafson, D.-K. Fu, H.-L. Wang, T. M. Swager, A. G. MacDiarmid, and A. J. Epstein, Phys. Rev. B **54**, 9180 (1996).
[64] J. Cornil, D. A. Dos Santos, X. Crispin, R. Silbey, and J. L. Bredas, J. Am. Chem. Soc. **120**, 1289 (1998).
[65] N. Verdal, J. T. Godbout, T. L. Perkins, G. P. Bartholomew, G. C. Bazan, and A. M. Kelley, Chem. Phys. Lett. **320**, 95 (2000).
[66] L. H. Chen, D. W. McBranch, H. L. Wang, R. Helgeson, F. Wudl, and D. G. Whitten, Proc. Natl. Acad. Sci. U.S.A. **96**, 12287 (1999).
[67] R. M. Jones, T. S. Bergstedt, D. W. McBranch, and D. G. Whitten, J. Am. Chem. Soc. **123**, 6726 (2001).
[68] B. S. Gaylord, S. Wang, A. J. Heeger, and G. C. Bazan, J. Am. Chem. Soc. **123**, 6417 (2001).
[69] J.-H. Hsu, W. Fann, P.-H. Tsao, K.-R. Chuang, and S.-A. Chen, J. Phys. Chem. A **103**, 2375 (1999).
[70] G. H. Gelinck, J. M. Warman, and E. G. J. Staring, J. Phys. Chem. **100**, 5485 (1996).
[71] I. D. W. Samuel, G. Rumbles, C. J. Collison, S. C. Moratti, and A. B. Holmes, Chem. Phys. **227**, 75 (1998).
[72] C. J. Collison, L. J. Rothberg, V. Treemaneekarn, and Y. Li, Macromolecules **34**, 2346 (2001).
[73] P.-G. deGennes, *Scaling Concepts in Polymer Physics* (Cornell University Press, Ithaca, 1979).
[74] Yu. B. Melinchenko and G. D. Wignall, Phys. Rev. Lett. **78**, 686 (1997).
[75] I. Borukhov, R. F. Bruinsma, W. M. Gelbart, and A. J. Liu, Phys. Rev. Lett. **86**, 2182 (2001).
[76] B. Y. Ha and A. J. Liu, Phys. Rev. Lett. **79**, 1289 (1997).
[77] D. H. Hu, J. Yu, and P. F. Barbara, J. Am. Chem. Soc. **121**, 6936 (1999).
[78] C. Y. Yang, F. Hide, M. A. Diaz-Garcia, A. J. Heeger, and Y. Cao, Polymer **39**, 2299 (1998).
[79] B. A. Weir, E. A. Marseglia, S. M. Chang, and A. B. Holmes, Synth. Met. **101**, 154 (1999).
[80] T-Q. Nguyen, B. J. Schwartz, R. D. Schaller, J. C. Johnson, L. F. Lee, L. H. Haber, and R. J. Saykally, J. Phys. Chem. B **105**, 5153 (2001).

[81] R. D. Schaller, L. F. Lee, J. C. Johnson, L. H. Haber, R. J. Saykally, J. Vieceli, I. Benjamin, T.-Q. Nguyen, and B. J. Schwartz, J. Phys. Chem. B (submitted).
[82] A. Dogariu, D. Vacar, and A. J. Heeger, Phys. Rev. B **58**, 10218 (1998).
[83] E. S. Maniloff, V. I. Klimov, and D. W. McBranch, Phys. Rev. B **756**, 1876 (1997).
[84] The $\sqrt{t}$ term in Eq. (1) accounts for the change in spatial distribution of the excitons as they annihilate each other over different distances. A similar model for exciton–exciton annihilation without this term is also often used. For more details on the use of both models to fit exciton–exciton annihilation dynamics, see Refs. 13, 82, and 83 as well as S. L. Dexheimer, in *Optical and Electronic Properties of Fullerenes and Fullerene-Based Materials*, edited by J. Shinar, Z. V. Vardeny, and Z. H. Kafafi (Dekker, New York, 2000), and references therein.
[85] The rate of exciton diffusion along the polymer backbone is much slower than the rate of exciton diffusion between chains; see T.-Q. Nguyen, J. Wu, V. Doan, B. J. Schwartz, and S. H. Tolbert, Science **288**, 652 (2000).
[86] Because errors in measuring the spot size and pulse energy at the sample make it difficult to precisely determine the excitation density in our experiments, the absolute values quoted for $\beta$ are likely accurate only to within a factor of 2. The relative values, however, are precise to within a few percent, and thus we are certain that the value of $\beta$ in the protonated film is twice as large as that in the neutral film. See Ref. 13 for more details about how $\beta$ is calculated from the data like those shown in Fig. 6.